Taylor & Francis
Taylor & Francis Group

Low-cost aerial photography for high-resolution mapping of hydrothermal areas in Yellowstone National Park

B. PLANER-FRIEDRICH*†‡, J. BECKER‡, B. BRIMER‡ and B. J. MERKEL‡
†Trent University, Environmental & Resource Studies Program, 1600 West Bank Drive, Peterborough, Ontario, Canada K9J 7B8
‡Technische Universität Bergakademie Freiberg, Department of Geology, Gustav-Zeuner-Str.12, 09599 Freiberg, Germany

A site-specific high-resolution aerial survey was conducted to map a status quo of two rapidly changing hydrothermal areas in Yellowstone National Park. A $2\,m^3$ helium balloon released to 50–80 m altitude served as a low-cost platform easy to launch and retract on a highly flexible operating schedule. Pictures were taken with a digital camera with automatic interval shutter release. Owing to the balloon's sensitivity towards wind and the limited possibility of controlling its accurate positioning, the acquired aerial pictures varied significantly in altitude, tilt, and orientation. Automatic stitching was possible in areas where nearly vertical pictures with sufficient overlap existed. Those aerial pictures with little overlap or taken at a highly oblique angle had to be manually post-processed based on temporary marked ground control points and additional tie points (total time for processing: 10–14 days) to obtain a final mosaic with minimal distortion $(0.4\,m \pm 0.3\,m)$ and an absolute accuracy of approximately 0.5 m. Ground resolution was better than 2 cm. Vegetation and hydrothermal feature classification, biological and redox zonations, water contents of mud pots, gas activity in hot springs as well as subaquatic sedimentation fans and hydrothermal vents could be outlined, providing a highly detailed thermal inventory for future change detection.

1. Introduction

Norris Geyser Basin currently is the most active hydrothermal area in Yellowstone National Park. After nine years of dormancy, its most prominent feature, 'Steamboat Geyser', the world's largest geyser, erupted in May 2000, again in April and September 2002, and in March and April 2003. Porkchop Geyser, dormant since 1989, has erupted in 2003, and a general trend of increasing spring and ground temperatures has been observed. Deformation maps inferred from satellite interferometric synthetic aperture radar delineate a $30 \times 40\,km$ large area of uplift at the northern rim of the Yellowstone caldera, underneath the Norris Geyser Basin ('Norris Uplift Anomaly') (Wicks *et al.* 2003). Pressure decrease caused by the inflation (125 mm from 1997 through 2002) and surface dilatation is most likely the trigger of the current increase in advective heat flow. A further phenomenon observed in the Norris Geyser Basin only is the 'annual hydrothermal disturbance', which occurs in late August to September as a result of decrease in the local

*Corresponding author. Email: brittaplaner@trentu.ca

potentiometric surface (White *et al.* 1988). It causes increased discharge of steam and water, significant temperature fluctuations, and increased turbidity in many springs, as well as sometimes small hydrothermal explosions. One area in the northern part of the Norris Geyser Basin, called Ragged Hills, has received special attention. It has only evolved in its hydrothermal activity since the mid-1990s when initially three small springs appeared in a 20×50 m area (Ball *et al.* 2002). Hydrothermal activity increased rapidly, especially in 1999, a year of significantly increased earthquake activity. By the end of 2000, the area of hydrothermal activity had grown to approximately 270 by 2150 m. Ever since, the hydrothermal features have changed rapidly in appearance, size, and activity.

Mapping such rapid changes in hydrothermal activity to record past and possibly predict future developments has become high priority both from a scientific viewpoint and for resource management. However, doing so by conventional ground survey methods at a sufficiently resolved scale yet over a sufficiently large area and within a minimum period of time proved impossible. A common alternative approach is remote sensing. Since the first aerial photos were taken from a manned, hot air balloon in 1858 by 'Nadar' (Gaspard-Félix Tournachon, documented in his *Mémoires du Géant, à terre et en l'air* in 1864), all kinds of manned and unmanned platforms ranging from satellites and aircrafts to low-flying platforms have been employed. For low-flying platforms, balloons (Palacio-Prieto and López-Blanco 1994, Kamada and Okabe 1998, Baker *et al.* 2004, Miyamoto *et al.* 2004), hot-air blimps (Ries and Marzolff 1997, Ries and Marzolff 2003), and kites (Boike and Yoshikawa 2003) have been used to obtain aerial photos for mapping temporal changes in soil and regolith morphology, mapping vegetation patterns on a river bar and in a wetland, monitoring gully-erosion rates, identifying sediment sources in semi-arid environments, and mapping periglacial morphology and vegetation, respectively. For research on emission of active volcanoes, sensors have been deployed on sturdy weather balloons at altitudes of several hundreds of metres to tens of kilometres, e.g. for aerosol particle counting (Watanabe *et al.* 2004). However, there is a gap in the literature about obtaining very-high-resolution, georectified, mosaicked aerial imagery for characterization and change detection in hydrothermal areas.

For the Norris Geyser Basin, colour aerial photos taken on 4 September 1986 (1:9600) and 22 September 1993 (1:20 000) are available from the Technical Information Center of the National Park Service. In a descriptive way, they document some of the larger hydrothermal changes. However, apart from their insufficient ground resolution, they are of no use for detailed mapping purposes without specific georectification. Black-and-white scanned aerial orthophotos exist for March 1997 from the National Aerial Photography Program (http://wgiac.state.wy.us/html/doqq75/44110.asp). Photos were taken from an aircraft altitude of approximately 20 000 feet above main terrain. Each photo is centred on a one-quarter section of a 7.5-minute USGS quadrangle. At a scale of about 1:40 000, the pixel resolution is about 1 m. For hydrothermal change detection, however, those aerial photos are insufficient because of their low resolution and irregular update frequency.

As a low-cost technique, small-format digital aerial photography from a tethered helium balloon was tested in the present study for its applicability and the interpretability of the resulting aerial map. A common criticism with small format aerial photography is the camera's geometric instability and limited precision and

accuracy (Warner and Carson 1991). This criticism becomes even more significant with digital cameras and their low-cost lenses. Often, it is impossible to obtain data about the inner orientation of the camera; thus, alternative camera calibration methods have been suggested (Zhang 2000). Obtaining aerial photos from a helium balloon poses additional challenges, since the flight path is barely controllable, the altitude varies significantly ($\pm 20\%$) with wind effects, and a spinning camera can produce aerial photos rotated up to $360°$ horizontally (yawing) and tilted up to $\pm 20°$ from the vertical axis (pitching and rolling). As part of the National Elevation Dataset a digital elevation model with a resolution of $10 \times 10\,m$ was available for the entire area of the Yellowstone caldera through the US Geological Survey EROS Data Center. However, because of its low ground resolution compared with the high-resolution aerial photos, the DEM was not sufficient as a basis for improving the processing of the aerial photos obtained. The present study was conducted in two hydrothermal areas in and just north of the Norris Geyser Basin and shows that it was still possible to obtain a final coloured, non-blurred photo mosaic of the hydrothermal areas with a ground resolution of about 2 cm and georectify it with minimal distortion ($0.4\,m \pm 0.3\,m$) and an absolute accuracy of about 0.5 m. The technique proved to be a useful tool to derive valuable information for characterization and change detection in the rapidly changing hydrothermal areas with minimal start-up material costs.

2. Methodology

The aerial photos were taken from a helium balloon platform over Ragged Hills, Norris Geyser Basin, around noon on 27 September and 1 October 2003. The area of interest is a relatively flat treeless plain at about 2280 m altitude ASL (maximum altitude differences 8 m) with a north-east–south-west extension of 500 m and a north-west–south-east extension of 150 m. The surrounding hills are at 2295 m ASL in the north-west and 2310 m ASL in the south-east ('Ragged Hills'). The second study area, West Nymph Creek Thermal Area, about 4 km north-west of the Norris Geyser Basin, is an as-yet little explored backcountry site. It was mapped around noon on 22, 24, 26, and 27 September 2004. The challenges in this second study area were larger altitude differences (altitude differences up to 50 m) as well as the separation of a northern, central, and southern hydrothermal group by a narrow, tree-covered drainage. Noon proved to be the best time for the aerial photography not only because of the high light illumination with little shadow effects but also because of the wind conditions. The earlier morning was generally even calmer, and in previous studies (Palacio-Prieto and López-Blanco 1994) enhanced aerial photography has been described with low-angle illumination, but increased amounts of steam rising from the hydrothermal features at colder temperatures made early-morning photography impossible in the present case. To obtain a high ground resolution for the final map, the operating altitude of the balloon was restricted to 50–80 m (160–260 feet) above ground. Unmanned aircraft operations below 500 ft do not require any permission by Federal Aviation Regulations in the US. A photo taken at 50 m altitude with the camera used (Canon Powershot G5) covers approximately $36 \times 58\,m$ on the ground, at 80 m altitude $58 \times 92\,m$ on the ground. The idea was thus to create a mosaic map covering the whole area from multiple georectified photos.

Georectification of an aerial image requires at least three ground control points with known coordinates for orientation; each further control point improves the

internal rectification. Crosses of red-and-white barricade tape (1 m length and 0.1 m width) served as temporary ground control points for the duration of the aerial survey. Cross-shaped markers were found to be superior for relocating the exact GPS position to the often-used rectangles (Miyamoto *et al.* 2004). Stones were used to hold the markers down on the ground. The raster with a total of 102 markers for Ragged Hills and 171 markers for West Nymph Creek Thermal Area was laid out in an equidistant 28×28 m grid as far as natural features permitted. Each aerial photo used for the later mosaic contained four to eight ground control points. The coordinates of the control points were determined by differential GPS (Trimble Pathfinder Pro XR) with 150 readings every second taken for each control point and processed by offline correction by a reference station in Bozeman. An estimated precision in the *x*- and *y*-direction of ± 0.5 m was achieved. Even better precision (± 0.03 m) in a shorter survey time can be achieved using a real-time kinematic (RTK) GPS. At Ragged Hills, 81 out of 102 ground control points were surveyed for comparison additionally by theodolite (LEICA TCR 307 reflectorless total station). Changes in the atmospheric conditions during the theodolite survey were taken into account by measuring the coordinates of one checkpoint at two times, at the beginning and at the end of the survey. The differences between the two measurements were 0.494 cm in the northing and 0.426 cm in the easting. The overall deviations between differential GPS and theodolite survey were 37 ± 49 cm in the northing and 61 ± 100 cm in the easting for 81 control points.

The latex balloon used as a low-flying platform was filled with $2 \, \text{m}^3$ of helium to a diameter of about 1.5 m (cost: approx. \$20 for the balloon plus \$70 for the helium). The maximum payload was 1.7 kg, the lifting capacity of 2000 l of helium ($1 \, l \cong 1$ g weight) minus the weight of the balloon itself. On all survey days, wind velocities were below $1.8 \, \text{m s}^{-1}$ (3.5 knots). At higher wind velocities, the balloon became extremely hard to control in both direction and altitude. Figure 1 shows the construction attached to the helium balloon. Two nylon tethering lines are directly attached to the clip closing the helium balloon. The total weight of the two tethering lines—each 100 m long—is about 0.5 kg. Two tethering lines were found superior compared with one for manoeuvring and positioning the camera without getting the tethering lines in the picture. The camera construction itself is also attached by four wires directly to the clip without connection to the tethering lines. Thus, when the balloon is dragged, the camera itself is not tilted. Alternatively, attaching a camera to converging lines of a parachute canopy wrapping the whole balloon has been suggested (Noli 1985). This has—apart from distributing the weight evenly over the balloon—the additional advantage of providing a backup system in case of balloon burst.

Two 0.75-m-long aluminium poles form the frame of the camera carrier construction. A 1-mm-thick intertwined wire around the four ends of the sticks gives additional stability to the construction; the wider the frame, the more stable the camera attached in its centre. The camera itself is fixed by a tripod screw to a metal plate in the centre of the aluminium frame. Two small, rubber stoppers support the weight of the camera. A wind metal plate for camera alignment with the prevailing wind direction was added to the construction to help orientate the camera in one direction. However, experience in the field showed that it had little positive effect. Tying two balloons together in 2004 increased not only uplift but also altitude stability significantly.

Optionally, a Garmin 12 GPS was attached to the balloon to track the balloon's flight path. Coordinates were saved in a 30-s interval. The overall accuracy of a GPS
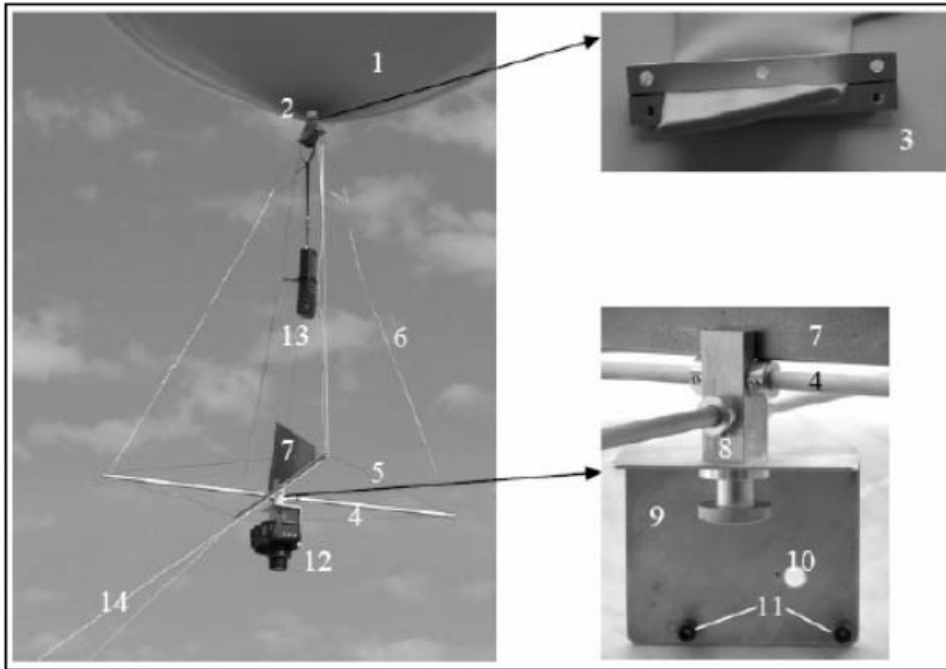
Figure 1. Home-made aluminium construction to support a digital camera and GPS mounted to the helium balloon (1=helium balloon, 2=plastic clips to seal balloon, 3=attachment for tethering lines and camera carrier construction, 4=aluminium poles, 5=wire to increase horizontal stability of frame of aluminium poles, 6=wires to attach camera carrier construction to (3), 7=a metal plate was added to the construction to align the camera along the prevailing wind direction, 8=middle axis to which metal plate (9) supporting the camera is attached, 10=tripod screw hole, 11=rubber stoppers to support camera weight, 12=digital camera Canon Powershot G5, 13=GPS GARMIN-12, 14=tethering lines).

receiver mainly depends on receiver, antenna, location, surrounding objects, satellite constellation status, and ionosphere conditions. Tests under comparable conditions showed that 50% of readings of the Garmin 12 GPS plot within a radius of about 4.5 m and 95% within a radius of 12 m. However, since the GPS receiver on a flying platform is continuously moving, averaging and the precision of a receiver has no impact on the result. Therefore, the GPS position of the camera was too fuzzy to improve the georectification of the final mosaic. GPS with WAAS (Wide Area Augmentation System) in operation may be a valuable option for today's surveys.

The camera used was a digital Canon Powershot G5 with a size of $121 \times 74 \times 70$ mm at a total weight of 0.46 kg, including a BP-511 Li-ion battery. It features a 1/1.8' five megapixel CCD sensor capturing 2592×1944 pixels. The camera comes with an infrared remote-controlled shutter release. However, the range is only about 5 m from the front remote sensor and 3 m from the side remote sensor. Often, unmanned remotely controlled platforms for aerial photography have a radio-controlled shutter release. However, that adds additional weight and has little advantage except when the platform and/or the camera can be positioned by remote control and a desired frame can be selected by a view-finder, e.g. in an additional video camera. This, however, increases weight and cost significantly. One advantage of the Canon Powershot is its integrated intervalometer function which enables two to 100 images to be taken at pre-set interval times of 1–60 min. One

other published application was found where the intervalometer function of a Canon Powershot S50 was used for taking aerial pictures 10–30 m above a saline sulfidic discharge area (Baker *et al.* 2004). Another study (Boike and Yoshikawa 2003) describes the application of an Olympus C2020 triggered by a 'DigiSnap 2000' remote-control module connected to the camera's serial port. With a baud rate of 19 200, the manufacturer (Harbortronics) claims successful shutter release with a cable as long as 700 feet (http://www.steves-digicams.com/2001_reviews/ digisnap2000.html#2200). However, the cable adds additional weight to the lifting platform. In our study, the integrated intervalometer function was used. The first image was shot on the ground, and the balloon was then released to its final altitude while the interval shooting session started at one image per minute. The shutter speed was set to 1/1000 or 1/2000 to minimize blurring through camera movement on the balloon. The camera has a 4 times optical zoom lens with a focal length of 7.2–28.8 mm (equivalent to 35–140 mm of a 35-mm film). No zoom was used for the present application. Focus was manually set to an infinite distance (7.188 mm digital=34.62 mm equivalent). Images were saved as .jpg files ('superfine compression'=ca 1.4 MB per picture). A total of 170 pictures were shot at Ragged Hills, 45 of which were used for the final mosaic. In the West Nymph Creek Thermal Area, 50 out of 260 aerial photos were selected.

The aerial photos were pre-processed, when necessary, for brightness, whiteness, and contrast with standard graphic software, imported as raster objects in the GIS software TNTmips version 6.8, 6.9, and 7.0 (MicroImages) and georectified to the Universal Transverse Mercator system (Zone 12, Date: North American 1983) with a plane projective geometric transformation. This transformation is commonly applied for non-vertical aerial images of relatively flat terrain and uses a perspective projection in contrast, for example, to affine models with an orthographic or parallel plane projection. The plane projective model requires a minimum of four nonlinear control points which were found on all of the individual aerial pictures. The georectified photos were then added one by one to the final mosaics. All overlap regions were manually checked, and tie points were used when the automated rigid transformations showed large geometric discontinuities. Tie points were manually added, identifying corresponding locations in a pair of overlapping images and enabled, e.g. to re-position drainage setoffs in the lower centimetre range.

The whole mosaic then had to be resampled to remove artefacts caused by the varying altitude of the balloon while pictures were being taken (50–80 m) and geometric distortions caused by topography (especially in the case of West Nymph Creek Thermal Area). Cubic convolution, which uses a 4×4 block of surrounding input cells to calculate an output cell value, was used as the preferred resampling method to obtain a smooth yet sharp mosaic. For resampling aerial photos taken over a relatively flat river bank area for channel movement studies, cubic convolution was also chosen as the best fit (Hughes *et al.* 2006). A disadvantage is the relatively high computational cost. A $\sin(x)/x$ resampler which uses 8×8 or 16×16 cell size windows and might thus result in even sharper and smoother images would have been 2–4 or 4–16 times slower than cubic convolution and was not applied. Less CPU-time intensive models are nearest-neighbour and bilinear interpolation. The nearest-neighbour model, which takes the single input pixel nearest to the transformed point as the resampled output pixel, was found to offset feature edges by distances up to half the input cell size. The output was rather jagged, probably because of the different rotations and scales of the input rasters.

Results for bilinear interpolation, which takes a weighted average of the four input pixels around the transformed point, were mainly similar to that of cubic convolution, but appeared slightly blurred. For the overlap, the uppermost raster in each overlap area was used for computing the output image. Other techniques like feathering, average, maximum, minimum, chessboard, or random mixing overlap the cell values by comparing or mathematically combining the corresponding cell values of the input images and leave less choice to the interpreter.

In the end, the combined mosaics were georectified once more using all 102 ground control points for Ragged Hills (171 for West Nymph Creek Thermal Area), because the manually added tie points and the resampling process led to a slight offset of the original coordinates. For this final georectification, piecewise affine was chosen as the warping model. Compared with the plane-projective model used for georeferencing the individual pictures, piecewise affine does not compute a global best-fit solution for the entire image but considers distortions that change significantly over small areas. Each control point is assumed to be in the correct position, and Delaunay triangulation is used for interpolation in between. Thus, a single distorted control point location only affects the immediately surrounding triangles. Piecewise affine could not be used for the initial georeferencing of the individual pictures because it requires at least six (ideally more) control points as opposed to four for the plane-projective model. If only those aerial pictures that had six or more control points initially were used, this would have reduced the number of usable pictures substantially.

In an effort to decrease the manual processing time, automation of the mosaicking process has been attempted. To remove radiometric distortions caused by camera lens distortion, the camera's internal calibration was determined using a planar checkerboard calibration image in Matlab (The MathWorks, Natick, MA). Information on focal length, principal point, skew, and distortion factors provided the basis for automatic rectification of the aerial pictures which took 15 min per picture using a Unix Dual Core 2*2.6-GHz computer. Maximum deviations of 50 cm were found between non-rectified and rectified pairs of images. Compared with the geometric distortions caused by tilt and rotation of the camera mounted on the balloon, the average observed radiometric distortions were very minor. Improvement on the final mosaic was not substantial enough to justify the additional time needed for lens calibration and to rectify 170 and 260 pictures for Ragged Hills and West Nymph Creek Thermal Area, respectively.

Automatic stitching, as opposed to manually georeferencing individual pictures and stitching them by additional tie points, was tried using the program PTGui 6.0.3 (New House Internet Services, Netherlands). This yielded quick and accurate results with little necessity for additional control points in areas where the aerial pictures were nearly vertical with sufficient overlap. Using a balloon as survey platform, however, yielded aerial pictures which were tilted up to $\pm 20°$ from the vertical axis (pitch and roll parameters) and showed any rotation from 0 to 360° between two images (yaw parameter), often with minimal overlap. In such areas, the automatic stitching algorithm was unable to detect control points or resulted in complete misalignment of individual pictures. Additionally, misalignment was encountered when the seam line crossed large uniform areas, such as the water surface of hydrothermal features or largely plain white alteration areas as in the north-eastern part of Ragged Hills. Adding some additional control points manually or removing individual pictures mostly resolved the problem but increased processing time.

3. Results

Figures 2 and 3 show the resulting mosaics for Ragged Hills and West Nymph Creek Thermal Area, respectively. Both Ragged Hills—a relatively flat, easily accessible, rectangular shaped area—and West Nymph Creek Thermal Area with a higher relief energy, hydrothermal areas intersected by narrow drainages, and dense tree coverage were successfully mapped in a final ground resolution of 2 cm per pixel. The absolute accuracy of the mosaic was mainly determined by the accuracy of the differential GPS (± 0.5 m) which could be further optimized (± 0.03 m) using an RTK-GPS as mentioned before. The relative error within the mosaic due to distortions was checked by comparing distances measured in the field with a measuring tape (relative error ± 0.05 m) to those measured digitally in the final mosaic (relative error=pixel size=± 0.02 m). Four sites with four ground control points each were selected, and the four side lengths and two diagonals were measured at each site. For the 24 measurements, an absolute average deviation of 0.4 ± 0.3 m (20 ± 15 pixels) and relative standard deviations from 0.1% to 4.6% (mean 1.3%) were determined. A previous study (Hughes *et al.* 2006) testing how the number and type of ground control points as well as order of transformation polynomial affect spatial accuracy demonstrated that aerial photos of a floodplain

Figure 2.   Final georectified mosaic of the Ragged Hills.

Figure 3.   Final georectified mosaic of the West Nymph Creek Thermal Area.

landscape (resolution 1 m) can be consistently georectified with 30 ground control points to an accuracy of ± 5 m (5 pixels) with a 10% chance of greater error. A wetland aerial survey of comparable resolution to our study (15 cm) showed (non-corrected) misalignments between two photographs of 1.5 m (10 pixel) (Miyamoto *et al.* 2004). Others (Palacio-Prieto and López-Blanco 1994) determined mean errors between field and digital distance measurements for their aerial photos with a pixel size between 4 and 15 cm of 2.3–28.3% before and 0.5–4.6% after georectification, which is comparable to our results.

Figure 4 shows how much more detailed information can be obtained from the new high-resolution aerial maps compared with the previously existing aerial images with a ground resolution of 1 m. The mosaics were used as basis to manually digitize a vector object with a highly detailed thermal inventory. Additional information from a thorough ground survey as well as existing and newly obtained chemistry data were added as databases and visualized in colour-coded sampling points, as pie charts or bar graphs. All information was compiled in digital atlases. TNTatlas, a free product from MicroImages, facilitates access to and distribution of the so-acquired data.

It has been suggested before that high-resolution aerial photography can efficiently be used to detect changes in dynamic environments. That includes not
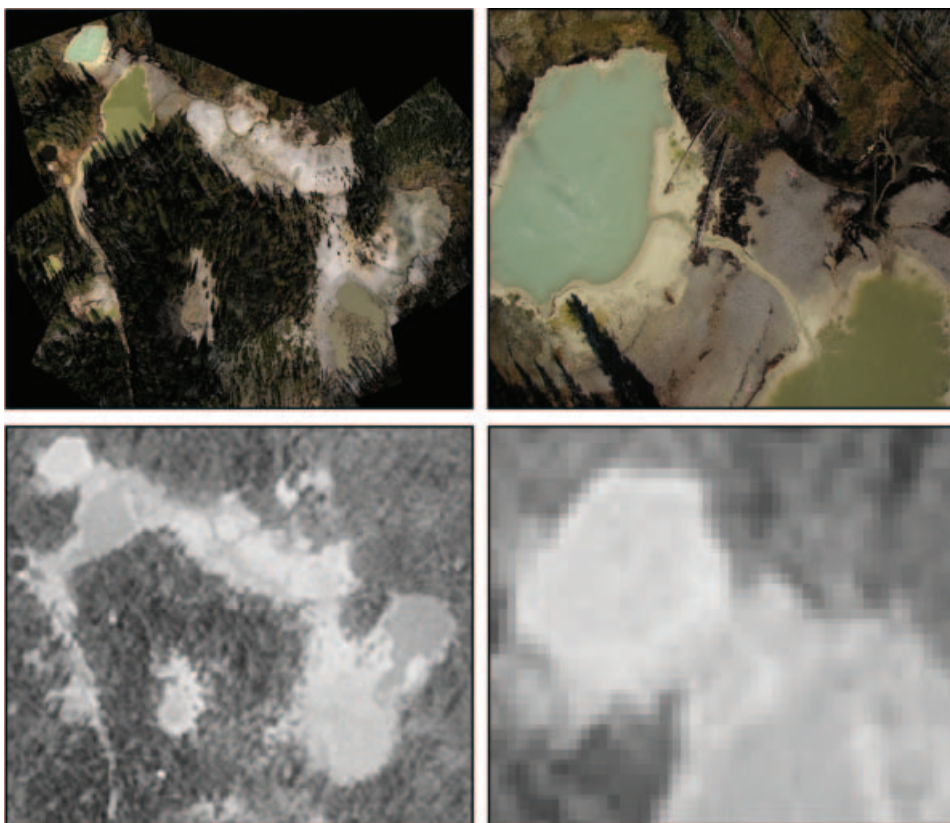
Figure 4.   Comparison between standard DOQQ aerial imagery with a ground resolution of 1 m and high-resolution (2 cm) aerial photos from this study, showing how much more detailed information can be retrieved from the latter.

only regular temporal changes such as seasonal vegetation but also more spontaneous events such as erosion after heavy rainfall or Fe-oxide colour change due to changing redox conditions, formation of salt efflorescence, etc. (Baker *et al.* 2004). In the present study, a global feature classification in meadows, wetlands, forests, deadfalls, hydrothermal alteration areas, explosion craters, geysers, clear and turbid hot springs, fumaroles, mudpots, and active and dried out drainage channels could be readily obtained (figure 5). Different colours and turbidity of the hydrothermal features are clearly distinguishable. The aerial photos could thus also be used to map features that are affected during the annual hydrothermal disturbance in the basin. Red iron-rich or milky-white silica-rich deposits can be outlined around the hot springs or along drainage channels (figure 5(*b*) and (*c*)). For the main discharge channel of Ragged Hills, draining Titanic hot spring to the north-east into One-Hundred-Springs Plain, a clear zonation from red iron-rich mats (0–40 m) over green algal (*Cyanidium caldarium*) mats (40–270 m) to grey-white clay deposits can be digitized from the aerial image (figure 5(*b*)). Previous studies on a smaller scale (up to 10 m from Beowulf spring (Langner *et al.* 2001, Inskeep *et al.* 2004)) have shown that this biological zonation represents not only a decrease in temperature but also significant changes in the distribution of redox-sensitive elements like S(–II)/S(VI), Fe(II)/Fe(III), and As(III)/As(V) ratios. Furthermore, sulfur-rich hot springs (like e.g. 'Orpiment Puddle' in Ragged Hills) with sizes of less than 1×1 m can be outlined on the aerial photos as intensive yellow features (figure 5(*d*)). According to ground observations, an increase in their number and size from 2002 to 2004 has been assumed but could not be quantified, yet. For the mudpots (mainly in West Nymph Creek Thermal Area), differences in water content can qualitatively be described, and future changes can be monitored (figure 5(*e*)). Figure 5(*f*) shows an aerial view from a wetland in the southern hydrothermal group of West Nymph Creek Thermal Area. Apart from the possibility of distinguishing different vegetation types and the main water courses within the wetland, the iron-rich sedimentation fan from an adjacent hot spring and even single basins or vents underneath the water surface can be delineated.

Overall, the helium balloon proved to be a very useful, low-cost platform for aerial surveillance of the hydrothermal features. The balloon was easily launched and landed, without the need for a runway. It works without any noise, which was especially valuable in the National Park with general aviation flight restrictions below 2000 ft above ground. The balloon platform is highly site-specific and very flexible both in the release altitude (and thus ground resolution of the final aerial imagery) and in its operating schedule. It can be rapidly deployed in response to triggering events and repeated easily. The Canon Powershot G5 digital camera produced pictures of sufficiently high quality with little distortion and had the additional advantages of a low weight and the optional intervalometer function. Remote-controlled release only has an advantage over the intervalometer function when the camera can be positioned and a single frame can be selected by an additional view-finder. This however, makes the whole equipment much more expensive. In a study from 1998 (Kamada and Okabe 1998), costs for such a setup were calculated to be US\$8500 for camera(s) and camera holder plus US\$3000 for the helium balloon (filled with 24 m^3 helium instead of 2 m^3!), whereas in 2003 our equipment came down to about US\$700 (US\$350 in 2006) for the camera and US\$50 for the balloon and construction.
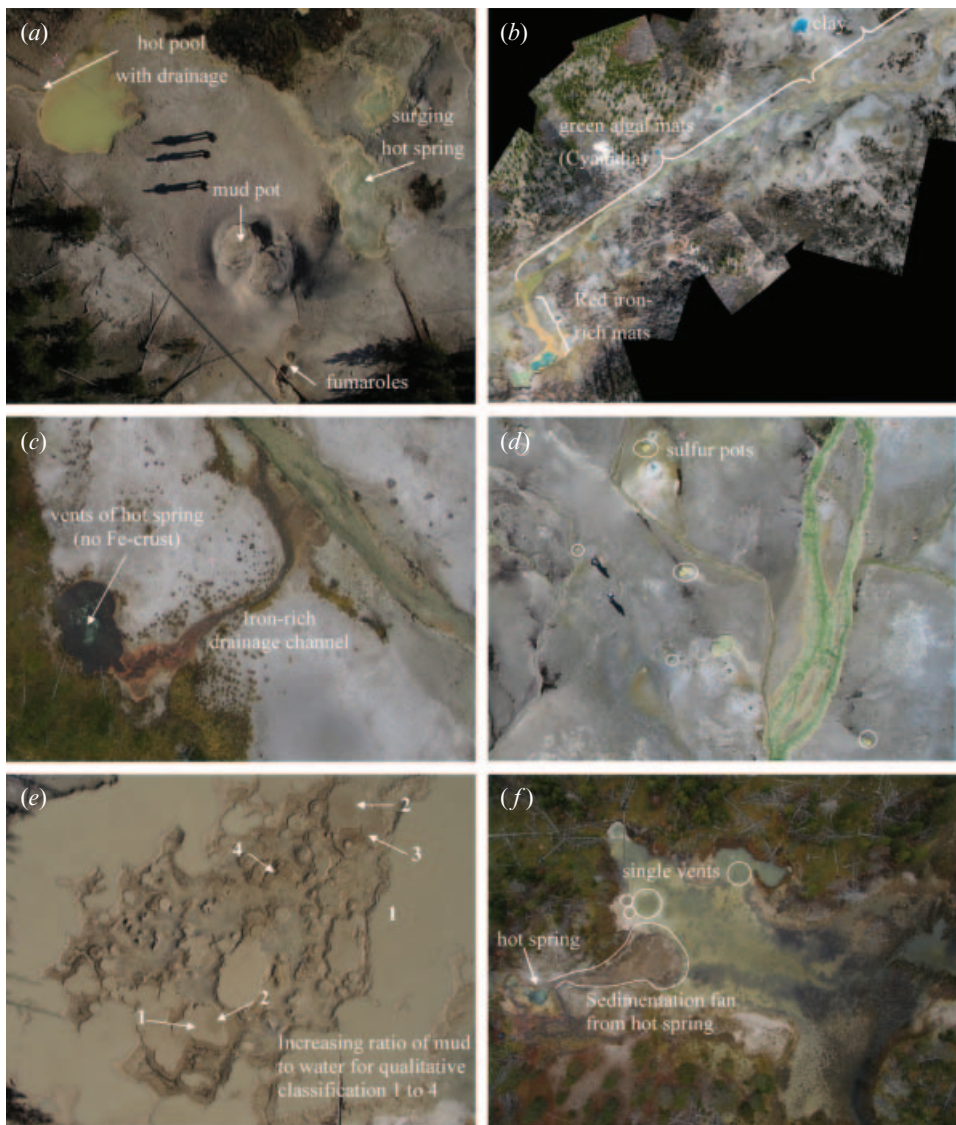
Figure 5. Examples for the potential of the high-resolution aerial maps in outlining important features of hydrothermal areas, (*a*) general hydrothermal feature classification (hot spring, hot pool, fumaroles and mudpot in West Nymph Creek Thermal Area, WNCTA). (*b*) Drainage channel in Ragged Hills with zonation from red iron-rich mats over green algal (*Cyanidium caldarium*) to gray-white clay deposits. (*c*) Unnamed spring in WNCTA showing a central vent surrounded by iron incrustations and the iron-rich drainage channel. (*d*) Sulfur puddles and drainage channel covered by Cyanidium in Ragged Hills. (*e*) Mudpots in WNCTA with distinguishably different water contents. (*f*) Wetland in the southern hydrothermal group of WNCTA showing different vegetation types, drainages, subaquatic vents, and basins, as well as an iron-rich sedimentation fan from an adjacent hot spring.

The disadvantages of the balloon clearly are its high sensitivity towards wind and little control over accurate positioning. Obstacles are potentially hazardous, even though the survey in West Nymph Creek Thermal Area showed that on a calm day,

it is also possible to manoeuvre the balloon through a small tree-covered drainage. The aerial photos obtained are far from being orthophotos. For many digital cameras, interior and exterior orientation are unknown, and the pictures vary both in horizontal orientation and in resolution due to varying balloon altitudes. Although they might be successfully georectified as shown, obviously, a single frame aerial photo taken with an expensive aerial camera from a greater height at the same ground resolution and orthorectified with a digital elevation model of comparable resolution is still preferable. A relatively large number of pictures have to be sorted and mosaicked to obtain the final map. The total amount of time for the optimized processing is estimated as 3 (5) man days for setting up and surveying the temporary ground control points, 2×2 h (4 times 2 h) for the flight itself, 6 (8) man days for georectifying the single images, and 4 (6) man days for creating the final optimized mosaic for a flat easily accessible area like Ragged Hills (estimates for a more scattered area such as West Nymph Creek Thermal Area in parentheses). Depending on the study area and pitch, yaw, and roll parameters of the aerial pictures (which in turn mainly depend on the wind conditions during the balloon survey), automatic stitching may be capable of replacing the manual mosaic processing and yield a mosaic within a few hours only. Fewer ground control points are necessary for final georeferencing of an already-assembled mosaic compared with individual pictures. On the downside, obviously, internal distortion will increase, and absolute accuracy will decrease compared with values reported for this study. Only the deployment of a more costly aerial survey platform, such as a remotely controlled blimp which can be launched to track a pre-programmed flight path, will help to obtain aerial pictures well aligned with an individually set overlap which can be mosaicked automatically with minimal distortion and a high accuracy.

In summary, whenever funds for material costs are limited, and flexibility of schedule is of priority, the balloon aerial survey can be highly recommended for mapping rapidly changing environments. Using this technique, a solid basis has been created for future high-resolution change detection in the two exemplary hydrothermal areas of Yellowstone National Park.

References
BAKER, A.K.M., FITZPATRICK, R.W. and KOEHNE, S.R., High resolution low altitude aerial photography for recording temporal changes in dynamic surficial environments, 2004, In *Regolith 2004*, I.C. Roach (Eds), pp. 21–25 (Bentley, Australia: Landscape Environments and Mineral Exploration Australia).
BALL, J.W., MCCLESKEY, R.B., NORDSTROM, D.K., HOLLOWAY, J.M. and VERPLANCK, P.L., 2002, *Water-Chemistry Data for Selected Springs, Geysers, and Streams in Yellowstone National Park, Wyoming, 1999–2000*. USGS, Open-File Report 02-382.
BOIKE, J. and YOSHIKAWA, K., 2003, Mapping of periglacial geomorphology using kite/balloon aerial photography. *Permafrost and Periglacial Processes*, **14**, pp. 81–85.

HUGHES, M.L., MCDOWELL, P.F. and MARCUS, W.A., 2006, Accuracy assessment of georectified aerial photographs: Implications for measuring lateral channel movement in a GIS. *Geomorphology*, **74**, pp. 1–16.

INSKEEP, W., MACUR, R., HARRISON, G., BOSTICK, B. and FENDORF, S., 2004, Biomineralization of As(V)-hydrous ferric oxyhydroxide in microbial mats of an acid-sulfate-chloride geothermal spring, Yellowstone National Park. *Geochimica et Cosmochimica Acta*, **68**, pp. 3141–3155.

KAMADA, M. and OKABE, T., 1998, Vegetation mapping with the aid of low-altitude aerial photography. *Applied Vegetation Science*, **1**, pp. 211–218.

LANGNER, H.W., JACKSON, C.R., MCDERMOTT, T.R. and INSKEEP, W.P., 2001, Rapid oxidation of arsenite in a hot spring ecosystem, Yellowstone National Park. *Environmental Science and Technology*, **35**, pp. 3302–3309.

MIYAMOTO, M., YOSHINO, K., NAGANO, T., ISHIDA, T. and SATO, Y., 2004, Use of balloon aerial photography for classification of Kushiro wetland vegetation, Northeastern Japan. *Wetlands*, **24**, pp. 701–710.

NOLI, D., 1985, Low-altitude aerial-photography from a tethered balloon. *Journal of Field Archaeology*, **12**, pp. 497–501.

PALACIO-PRIETO, J. and LÓPEZ-BLANCO, J., 1994, Using video imagery for gully erosion evaluation. *Zeitschrift für Geomorphologie*, **38**, pp. 33–43.

RIES, J. and MARZOLFF, I., 2003, Monitoring of gully erosion in the Central Ebro Basin by large-scale aerial photography taken from a remotely controlled blimp. *Catena*, **50**, pp. 309–328.

RIES, J.B. and MARZOLFF, I., 1997, Identification of sediment sources by large-scale aerial photography taken from a monitoring blimp. *Physics and Chemistry of the Earth*, **22**, pp. 295–302.

WARNER, W. and CARSON, W., 1991, Improving interior orientation for a small standard camera. *Photogrammetric Record*, **13**, pp. 909–916.

WATANABE, M., IWASAKA, Y., SHIBATA, T., HAYASHI, M., FUJIWARA, M. and NEUBER, R., 2004, The evolution of Pinatubo aerosols in the Arctic stratosphere during 1994–2000. *Atmospheric Research*, **69**, pp. 199–215.

WHITE, D.E., HUTCHINSON, R.A. and KEITH, T.E.C., 1988, The geology and remarkable thermal activity of Norris Geyser Basin, Yellowstone National Park, Wyoming. *USGS Professional Paper 1456*.

WICKS, C., THATCHER, W. and DZURISIN, D., 2003, Stress transfer, thermal unrest, and implications for seismic hazards associated with the Norris uplift anomaly in Yellowstone National Park. *Eos Transactions AGU, Fall Meeting Supplement Abstract G31B-0714*, **84**, pp. F500.

ZHANG, Z., 2000, A flexible new technique for camera calibration. *IEEE Transactions on Pattern Analysis and Machine Intelligence*, **22**, pp. 1330–1334.